32-37
82139
16 p.

THE AVOIDANCE OF SATURATION LIMITS IN MAGNETIC BEARING SYSTEMS DURING TRANSIENT EXCITATION*

235603

Neil K. Rutland, Patrick S. Keogh and Clifford R. Burrows
School of Mechanical Engineering
University of Bath
Bath BA2 7AY, UK

SUMMARY

When a transient event, such as mass loss, occurs in a rotor/magnetic bearing system, optimal vibration control forces may exceed bearing capabilities. This will be inevitable when the mass loss is sufficiently large and a conditionally unstable dynamic system could result if the bearing characteristics become non-linear. This paper provides a controller design procedure to suppress, where possible, bearing force demands below saturation levels whilst maintaining vibration control. It utilizes H_∞ optimisation with appropriate input and output weightings. Simulation of transient behaviour following mass loss from a flexible rotor is used to demonstrate the avoidance of conditional instability. A compromise between transient control force and vibration levels was achieved.

INTRODUCTION

Magnetic bearings are being used in increasing numbers in rotating machinery applications, both for the support of static loads and for the control of rotor vibration. However, the advantages of negligible frictional heating and wear are offset against the disadvantage of reduced load carrying capacity when compared with conventional bearings. Also, most applications are limited to relatively small rotors that are rigid in the sense that the rotational speed remains below the first rotor bending mode frequency.

Maximum force characteristics of a magnetic bearing are constrained by material saturation limits.

* **Work done under EPSRC Grant GR/J15575**

When such a bearing forms a component in an active rotor dynamic system, the associated controller is invariably designed on the assumption that the system behaves in a linear manner. Also, most industrial implementations configure magnetic bearings to act as decentralised springs and viscous dampers. Nonetheless, significant research progress has been made towards improved controller designs. An open loop technique for the control of steady synchronous vibration is now well established (ref. 1). The feedforward concept has been developed further (refs 2, 3) and applied to a turbo expander. Interest in the dynamic behaviour of synchronous vibration amplitudes has led to the control of transient rotor vibration through relatively slow acting closed loop controllers that utilise open loop influence coefficients (refs 4-8). Recent research published in the open literature has been directed towards the development of higher order centralised state space controllers (refs 9, 10). However, the non-linear influences of bearing saturation on controller design have received only limited attention.

During a rotor mass loss event, the following situations may arise during the transient rotor vibration response:

(a) The rotor dynamic system remains linear, without magnetic bearing saturation.
(b) The rotor dynamic system becomes non-linear, without magnetic bearing saturation.
(c) The magnetic bearing saturates with no possibility of the system returning to a linear steady state.
(d) The magnetic bearing saturates, though the system may have a linearly stable steady state.

For example, in case (c), the mass loss may be so large that the magnetic bearing cannot deliver sufficient control force and contact is made with emergency bearings. In cases (b) and (d), the controller design is important. A deficient controller for case (d) could result in a long period of saturation or even an unacceptable limit cycle response. Alternatively, a well designed controller would limit the transient saturation period. The proposition of the present paper is that the saturation time may be eliminated so that the controller ensures that case (d) is avoided completely.

NOMENCLATURE

A	system matrix
B_f , B_u	disturbance force, control force distribution matrices
c_d	derivative feedback gain
C_e , C_y , C_z , C_{zq}	coefficient matrices
$\boldsymbol{e}$, $\boldsymbol{e}_1$	control variable vectors
E_f , E_u	disturbance force, control force distribution matrices
$\boldsymbol{f}(t)$, $\boldsymbol{F}(s)$	vector of rotor external disturbance forces (time, Laplace domain)
$H(s)$	vibration controller transfer function matrix
$\boldsymbol{i}_c$	vector of magnetic bearing control currents
J	rotor gyroscopic matrix
k_p	proportional feedback gain
K	rotor stiffness matrix
k_i , k_z	magnetic bearing current, displacement coefficients
$\boldsymbol{m}^+$, $\boldsymbol{m}^-$	mass-eccentricity vectors
M	rotor mass matrix
$\boldsymbol{n}(t)$, $\boldsymbol{N}(s)$	vector of measurement errors (time, Laplace domain)
$\boldsymbol{q}$	vector of rotor lateral displacements and angular deflections
s	Laplace transform variable
t	time
T_{ef}, T_{uf}, T_{en}, T_{un}	closed loop transfer function matrices
$\boldsymbol{u}(t)$, $\boldsymbol{U}(s)$	control force vector (time, Laplace domain)
W_e, W_f, W_n, W_u	weighting function matrices
$\boldsymbol{x}$	state vector ($\boldsymbol{x} = [\boldsymbol{q}^T, \dot{\boldsymbol{q}}^T]^T$)
$\boldsymbol{y}(t)$, $\boldsymbol{Y}(s)$	vector of rotor displacements at transducer locations (time, Laplace domain)
$\boldsymbol{z}(t)$, $\boldsymbol{Z}(s)$	vector of rotor lateral displacements at magnetic bearings (time, Laplace domain)
τ	time constant
ω	frequency
Ω	rotational speed

SYSTEM DYNAMIC BEHAVIOUR

A project is being undertaken at the University of Bath to investigate vibration controller designs for flexible rotor systems. A rig has been constructed and the schematic form is shown in figure 1. It consists of a flexible rotor mounted on two magnetic bearings. The rotor was designed to have a mass of 100 kg with first and second rotor bending modes at around 26 Hz and 66 Hz respectively. A finite element rotor model leads to a discretized linear rotor dynamic system equation having the form

$$M\ddot{\boldsymbol{q}} + \Omega J\dot{\boldsymbol{q}} + K\boldsymbol{q} = E_f\boldsymbol{f} + E_u\boldsymbol{u} \tag{1}$$

Each magnetic bearing consists of two opposing pole pairs arranged at 45° to the vertical. The coils are powered by current amplifiers and, assuming a linear relation, the bearing control forces on the rotor are given by

$$\boldsymbol{u} = k_i\boldsymbol{i}_c + k_z\boldsymbol{z} \tag{2}$$

where

$$\boldsymbol{z} = C_{zq}\boldsymbol{q} \tag{3}$$

It follows that the system behaviour is governed by

$$M\ddot{\boldsymbol{q}} + \Omega J\dot{\boldsymbol{q}} + (K - E_u k_z C_{zq})\boldsymbol{q} = E_f\boldsymbol{f} + E_u k_i\boldsymbol{i}_c \tag{4}$$

For control design purposes, equation (4) is converted to the first order state space form

$$\begin{aligned} \dot{\boldsymbol{x}} &= A\boldsymbol{x} + B_f\boldsymbol{f} + B_u\boldsymbol{u} \\ \boldsymbol{y} = C_y\boldsymbol{x} \quad , \quad \boldsymbol{z} &= C_z\boldsymbol{x} \quad , \quad \boldsymbol{e} = C_e\boldsymbol{x} \end{aligned} \tag{5}$$

Here, $\boldsymbol{y}$ is a vector of lateral displacements of the rotor at the outer disks and magnetic bearings, corresponding to displacement transducer locations. The magnetic bearing force components $\boldsymbol{u}$ are to be used for levitation and vibration control. In order that the vibration control performance can be defined, the vector $\boldsymbol{e}$ is chosen to consist of variables that are to be minimised. In the Laplace transform domain the magnetic bearing forces are written as

$$\boldsymbol{U}(s) = H(s)\boldsymbol{Y}(s) - (-k_z + k_p + sc_d/(1+\tau s))\boldsymbol{Z}(s) \qquad (6)$$

where the levitation components consist of a practical implementation of proportional and derivative control.

A block diagram of the rotor/magnetic bearing system is shown in figure 2, which includes measurement noise and a reference position vector for the rotor at the bearings. Bearing saturation is also incorporated in figure 2 with the simple limiter on $\boldsymbol{u}$. It is now evident that, although the linear system may be stable, the non-linear system may only be conditionally stable. For example, mass loss from the rotor can be represented by a step change in the unbalance condition by

$$\boldsymbol{f}(t) = \begin{cases} \mathbf{0} & , \quad t \le 0 \\ \Omega^2 \boldsymbol{m}^+ e^{i\Omega t} + \Omega^2 \boldsymbol{m}^- e^{-i\Omega t} & , \quad t > 0 \end{cases} \qquad (7)$$

If the level of mass loss, represented by a norm of $\boldsymbol{m}^+$, is sufficiently small, the saturation limits will not be reached. Otherwise, an amplitude dependent response is likely and it is in this case that the vibration controller $H(s)$ can be used to influence the region of linear behaviour.

The system dynamic characteristics without vibration control ($H(s) = 0$) are evident from the steady synchronous unbalance responses of figure 3. The system unbalance corresponded to a nominal 10 g mass on the outer rim of the non-driven end disk with low/high values of the derivative gain. In figure 3(a), rigid body modes are apparent at around 45 rad/s. First order rotor flexure (164 rad/s) has a sharp response since the bearings are close to vibration nodes. The other critical speed involves second order rotor flexure around 420 rad/s and the broader peak indicates greater modal damping and controllability. In figure 3(b), modes involving rigid body rotor motion are well damped and do not exhibit any peaks in the response curves. The increased derivative gain has little effect on the first rotor flexural frequency, in contrast to the significant reduction of the second rotor flexural critical speed.

Mass loss simulations at a speed $\Omega = 500$ rad/s are shown in figure 4, starting from a perfect balance condition and with a mass of 60 g removed from the non-driven end disk at time $t = 0$.

Bearing saturation and clearance limits were not set so that the system remained linear. For low damping, the rotor displacement response at the non-driven end bearing exhibits transient responses of the critical speed modes. The rigid body response is significant and in any practical system the rotor would collide with emergency retainer bearings for displacements amplitudes above around 1mm. The high damping case of figure 4(b) reduces the rotor overshoot, though at the expense of substantially increased control forces. With the inclusion of control force limits of (-1700, 1000) N, biased by static loading, saturation is bound to occur in the high damping case. The simulated results are shown in figure 5, though still without clearance limits. The rotor responses at the bearings suffer from drift when compared with figure 4(b). Of course, in a practical system, the rotor would collide with an emergency bearing at the driven end magnetic bearing. Clearly, transient vibration control is not effective due to the passive configuration of the magnetic bearings.

VIBRATION CONTROLLER DESIGN

To define the level of vibration control, the variables in $\boldsymbol{e}$ were chosen to consist of lateral rotor velocities at the end disks and magnetic bearing locations, coincident with the measurement locations. Without stating the precise details, it is clear from figure 2 that a closed loop transfer function relation exists to relate the external disturbances to the control variables:

$$\boldsymbol{E}(s) = [\,T_{ef}(H;s)\,W_f(s)\,,\,T_{en}(H;s)\,W_n(s)\,]\begin{bmatrix} W_f(s)^{-1}\boldsymbol{F}(s) \\ W_n(s)^{-1}\boldsymbol{N}(s) \end{bmatrix} \tag{8}$$

The weighting $W_f(s)$ was selected as a diagonal matrix with a frequency response characteristic that recognises the nature of mass loss unbalance forcing. Singular value bode plots are shown in figure 6. The weighting $W_n(s)$ reflects the level of anticipated measurement noise and was chosen to have a flat spectrum of small amplitude. A basis on which to evaluate the controller is through the H_∞ optimisation problem

$$\underset{H}{\textit{minimise}}\ \|[\,T_{ef}(H;s)\,W_f(s)\,,\,T_{en}(H;s)\,W_n(s)\,]\|_\infty \tag{9}$$

However, this optimisation provides no means of accounting for the bearing saturation limits since it

assumes that unconstrained levels of control force are available.

To overcome the saturation problem, the control force vector $\boldsymbol{u}$ is now included in the control variables:

$$\boldsymbol{e}_1 = \begin{bmatrix} \boldsymbol{e} \\ \boldsymbol{u} \end{bmatrix} \tag{10}$$

A revised version of the closed loop system given by equation (8) is

$$\begin{bmatrix} W_e(s)\boldsymbol{E}(s) \\ W_u(s)\boldsymbol{U}(s) \end{bmatrix} = \begin{bmatrix} W_e(s)T_{ef}(H;s)W_f(s) & W_e(s)T_{en}(H;s)W_n(s) \\ W_u(s)T_{uf}(H;s)W_f(s) & W_u(s)T_{un}(H;s)W_n(s) \end{bmatrix} \begin{bmatrix} W_f(s)^{-1}\boldsymbol{F}(s) \\ W_n(s)^{-1}\boldsymbol{N}(s) \end{bmatrix} \tag{11}$$

with the H_∞ optimisation

$$\underset{H}{minimise} \left\| \begin{bmatrix} W_e(s)T_{ef}(H;s)W_f(s) & W_e(s)T_{en}(H;s)W_n(s) \\ W_u(s)T_{uf}(H;s)W_f(s) & W_u(s)T_{un}(H;s)W_n(s) \end{bmatrix} \right\|_\infty \tag{12}$$

Here the weightings $W_e(s)$ and $W_u(s)$ are introduced to allow design influences on control performance and control force respectively.

For the present problem, the rotor was modelled using 12 beam elements, including shear deformation. The levitation parameters were set at $k_p = 1.05\ k_z$, $c_d = 7.5\times10^3$ Ns/m and $\tau = 10^{-3}$ s to produce well damped low frequency rigid body modes without undue influence on the rotor flexural modes. The following weighting forms were arrived at after an iterative process to achieve required levels of vibration attenuation and control force output:

$$W_n(s) = 10^{-8}I \quad , \quad W_e(s) = I \quad , \quad W_u(s) = 10^{-4}I \tag{13}$$

In practice, some shaping would also be applied to these weightings in order that problems such as spillover may be avoided. A controller $H(s)$ may be determined in state space form using standard algorithms. For numerical efficiency, dominant mode techniques were employed to reduce the full

order 104 states rotor model to a 24th order state space model.

The significance of the revised vibration controller is shown in the simulated mass loss plots of figure 7. The rotational speed and mass loss correspond with those of figures 4 and 5. It is seen that synchronous steady state vibration levels are reduced below those of the high damping case in figure 4(b), yet magnetic bearing forces are now within saturation limits. There is an initial transient response involving mainly rigid body motion, though the vibration amplitudes would be well within clearance limits. Any attempt to reduce this transient would require increased transient control force levels. Thus a compromise between magnetic bearing saturation and clearance constraints is always necessary. There is scope for further design to influence steady state force components with alternative weighting functions, but the consideration of this paper has been focused on the transient behaviour. Some generalisation for mass losses at different locations and over a range of rotational speeds is also possible.

CONCLUSIONS

This paper has been used to show that there are circumstances in which vibration control may be achieved without magnetic bearing saturation in a rotor dynamic system. One of the consequences of this is that conditional system instability, caused by non-linear bearing behaviour, may be overcome. However, the ultimate level of achievable vibration control will still depend on the saturation limits and large unbalance conditions will result in significant residual vibration amplitudes. In particular, if the magnetic bearings are situated close to vibration nodes, low controllability will prevent significant reduction around certain critical speeds.

The control design included H_∞ optimisation to minimise both vibration responses and control force levels. Mass loss simulations were used to demonstrate the avoidance of saturation during transient conditions. The success of the method depends on a judicious choice of weighting functions appropriate to the anticipated levels of mass loss that are likely to occur. The weighting functions must be normalised to enable the optimisation problem to achieve desired performance levels. If the mass loss is greater than the levels accounted for in the design, bearing saturation may still occur.

REFERENCES

1. Burrows, C.R. and Sahinkaya, M.N.: Vibration Control of Multi-Mode Rotor Bearing Systems. *Proc.R.Soc.Lond.*, A386, 1983, pp. 77-94.
2. Larsonneur, R., Siegwart, R. and Traxler, A.: Active Magnetic Bearing Control Strategies for Solving Vibration Problems in Industrial Rotor Systems. *Proceedings (IMechE) of the Fifth International Conference on Vibrations in Rotating Machinery*, Bath, UK, September 7-10, 1992, pp. 83-90.
3. Larsonneur, R. and Herzog, R.: Feedforward Compensation of Unbalance: New Results and Experiences. *IUTAM Symposium on the Active Control of Vibration*, Bath, UK, September 8-11, 1994, pp. 45-52.
4. Berry, T., Burrows, C.R., and Keogh, P.S.: Active Control of Synchronous and Transient Vibration with Minimal System Modelling. ASME Winter Annual Meeting, New Orleans, paper 93-WA/DSC-4, 1993.
5. Knospe, C., Hope, R., Fedigan, S., and Williams, R.: New results in the Control of Rotor Synchronous Vibration. *Proceedings of the Fourth International Symposium on Magnetic Bearings*, Zurich, Switzerland, August 23-26, 1994, pp. 119-124.
6. Knospe, C., Hope, R., Fedigan, S., and Williams, R.: Experiments in the Control of Unbalanced Response using Magnetic Bearings. *Mechatronics*, vol. 5, no. 4, 1995, pp. 385-400.
7. Rutland, N.K., Keogh, P.S., and Burrows, C.R.: Comparison of Controller Designs for Attenuation of Vibration in a Rotor-Bearing System under Synchronous and Transient Conditions. *Proceedings of the Fourth International Symposium on Magnetic Bearings*, Zurich, Switzerland, August 23-26, 1994, pp. 107-112.
8. Shafai, B., Beale, S., LaRocca, P., and Cusson, E.: Magnetic Bearing Control Systems and Adaptive Force Balancing. *IEEE Control Systems*, vol. 14, no. 2, 1994, pp. 4-13.
9. Herzog, R. and Bleuler, H.: On Achievable H^{∞} Disturbance Attenuation in AMB Control. *Third International Symposium on Magnetic Bearings*, Washington D.C., 1992.
10. Keogh, P.S., Mu, C., and Burrows, C.R. Optimized Design of Vibration Controllers for Steady and Transient Excitation of Flexible Rotors. *Proc.I.Mech.E.Part C*, 1995, pp. 155-168.

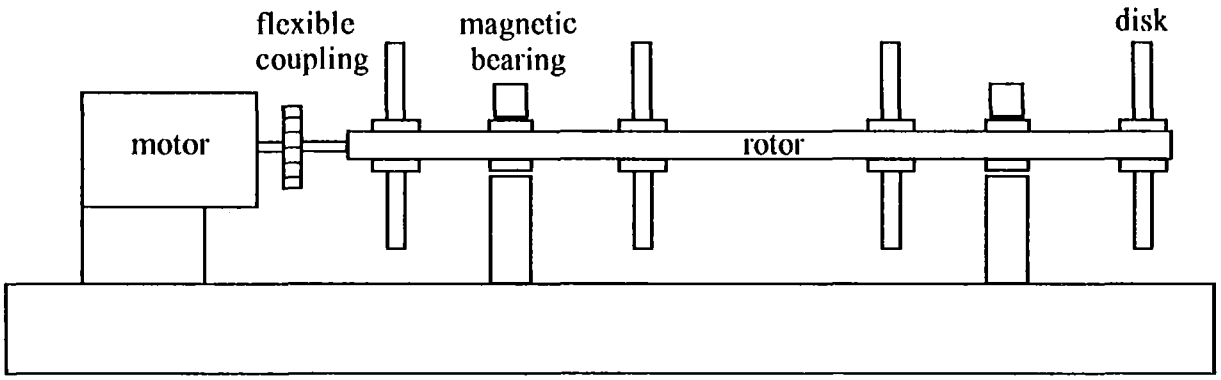

Figure 1. Schematic diagram of rotor / magnetic bearing system.
The steel rotor is 2m long with a shaft diameter of 50mm.
Disks are of 250mm diameter and 35mm wide.

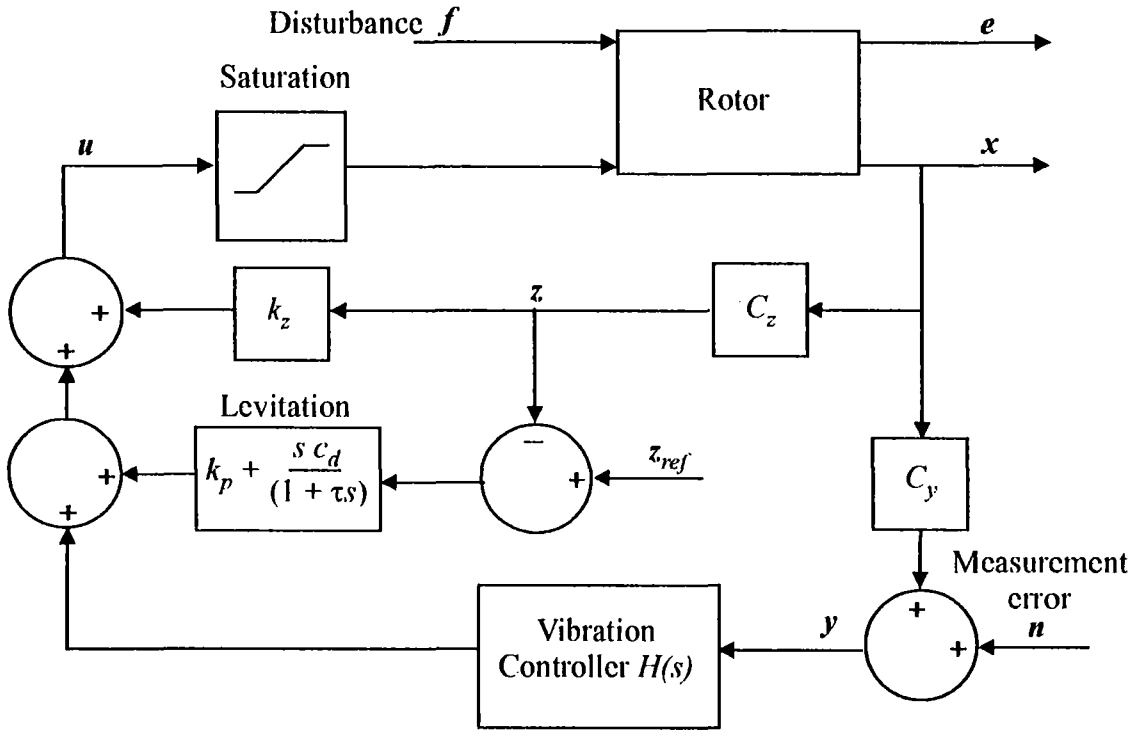

Figure 2. Block diagram of system including levitation and vibration control.

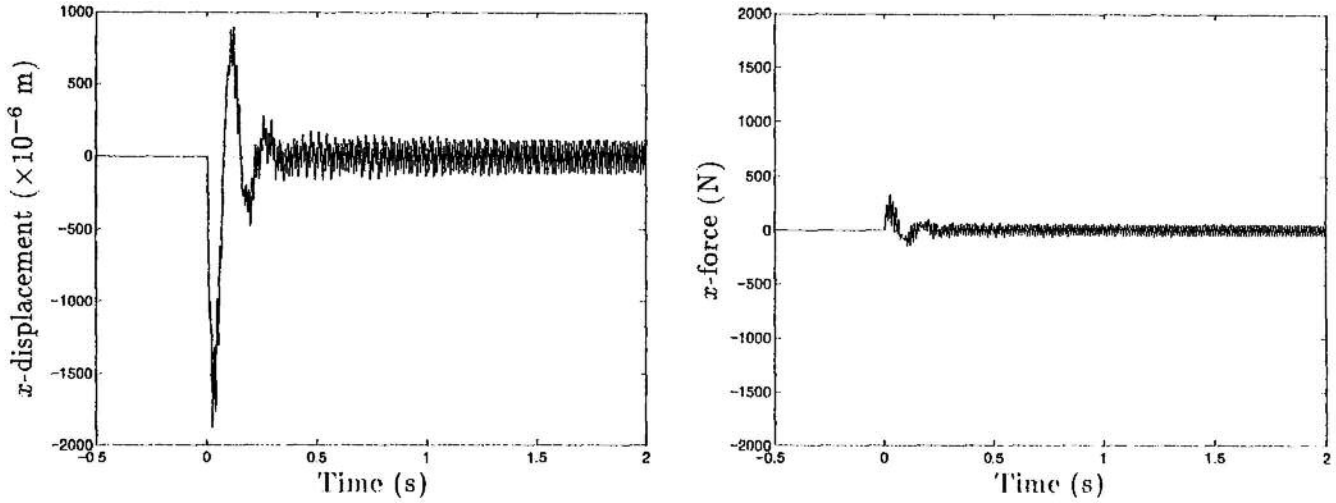

(a) Low damping ($c_d = 10^3$ Ns/m)

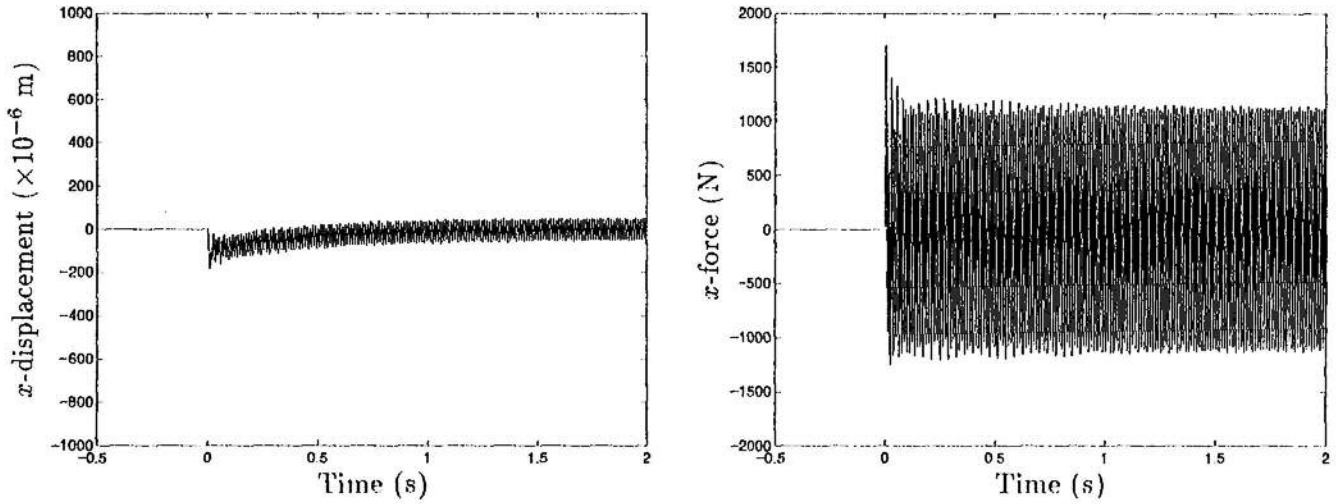

(b) High damping ($c_d = 5 \times 10^4$ Ns/m)

Figure 4. Mass loss simulations at a speed $\Omega = 500$ rad/s with a 60 g mass removed from the non-driven end disk rim in the x direction (45° to vertical against rotation) at $t = 0$ ($k_p = 1{\cdot}05k_z$, $k_z = 2{\cdot}05 \times 10^6$ N/m, $\tau = 10^{-3}$ s). Vibration components of rotor amplitude and bearing force are shown at the non-driven end magnetic bearing. Saturation and clearance limits were not set. The vibration controller of figure 2 is not present.

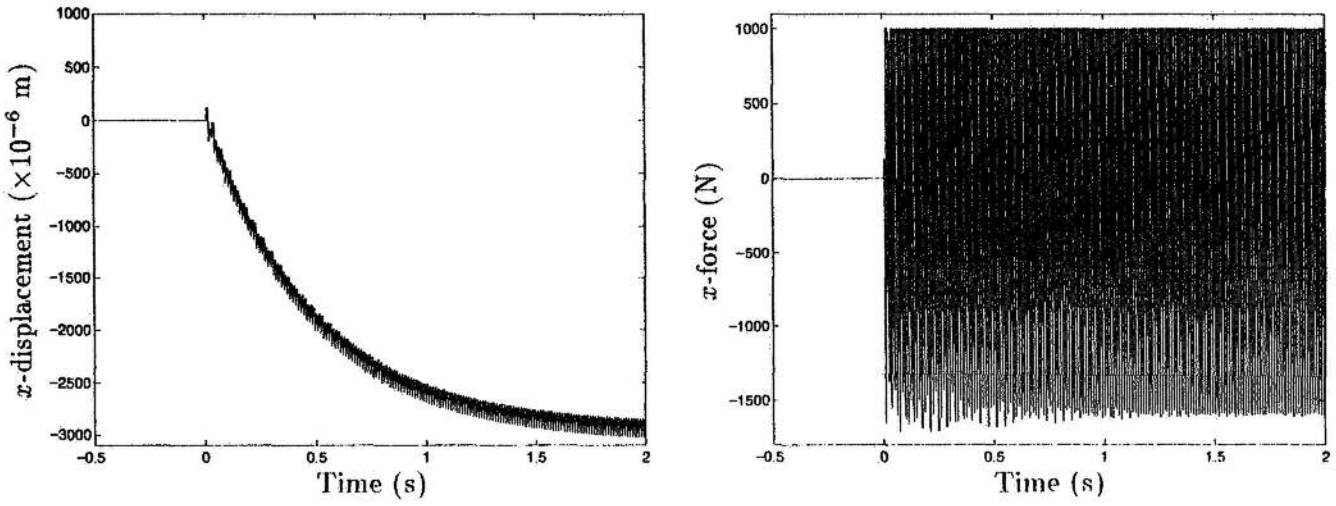

(a) Driven end magnetic bearing

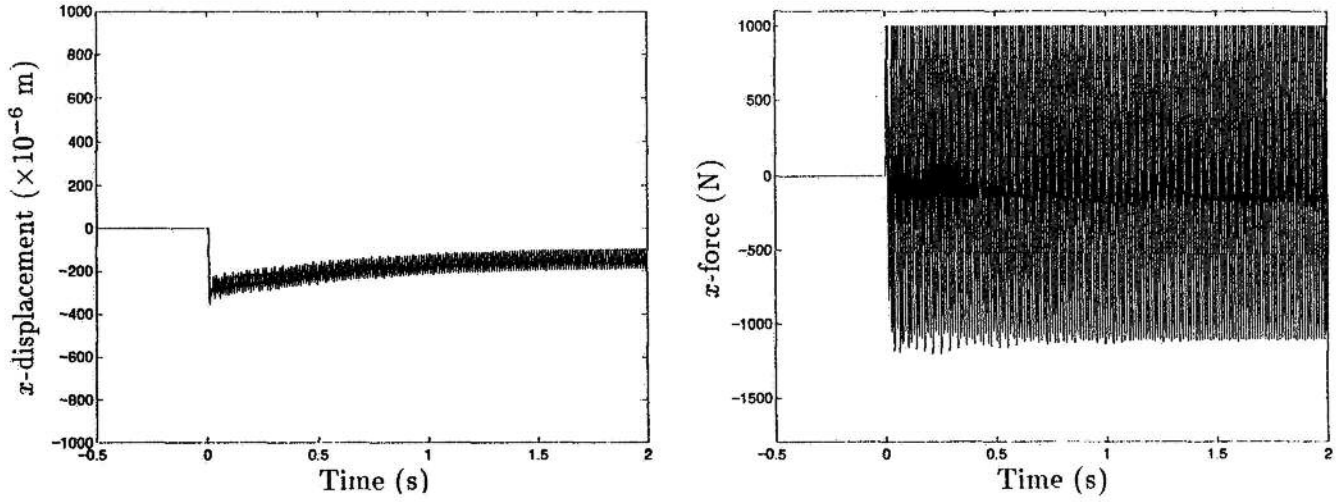

(b) Non-driven end magnetic bearing

Figure 5. Mass loss simulations at a speed $\Omega = 500$ rad/s with a 60 g mass removed from the non-driven end disk rim in the x direction at $t = 0$ ($k_p = 1{\cdot}05k_z$, $c_d = 5 \times 10^4$ Ns/m, $k_z = 2{\cdot}05 \times 10^6$ N/m, $\tau = 10^{-3}$ s). Vibration components of rotor amplitude and bearing force are shown at the magnetic bearings. Saturation force limits were set at 1000 and -1700 N. The vibration controller of figure 2 is not present.

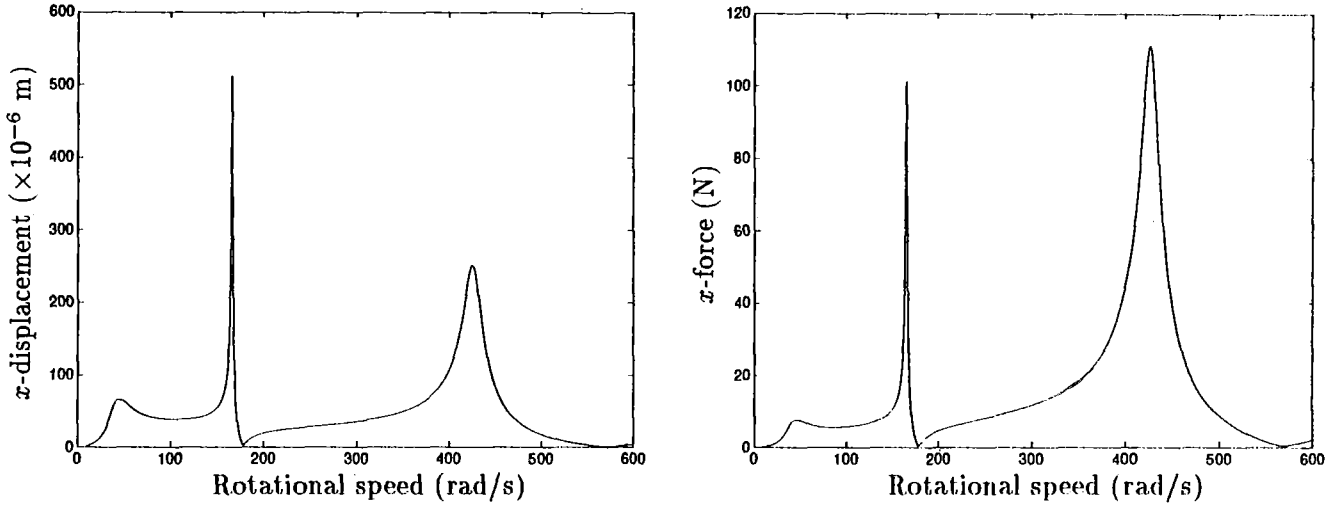

(a) Low damping ($c_d = 10^3$ Ns/m)

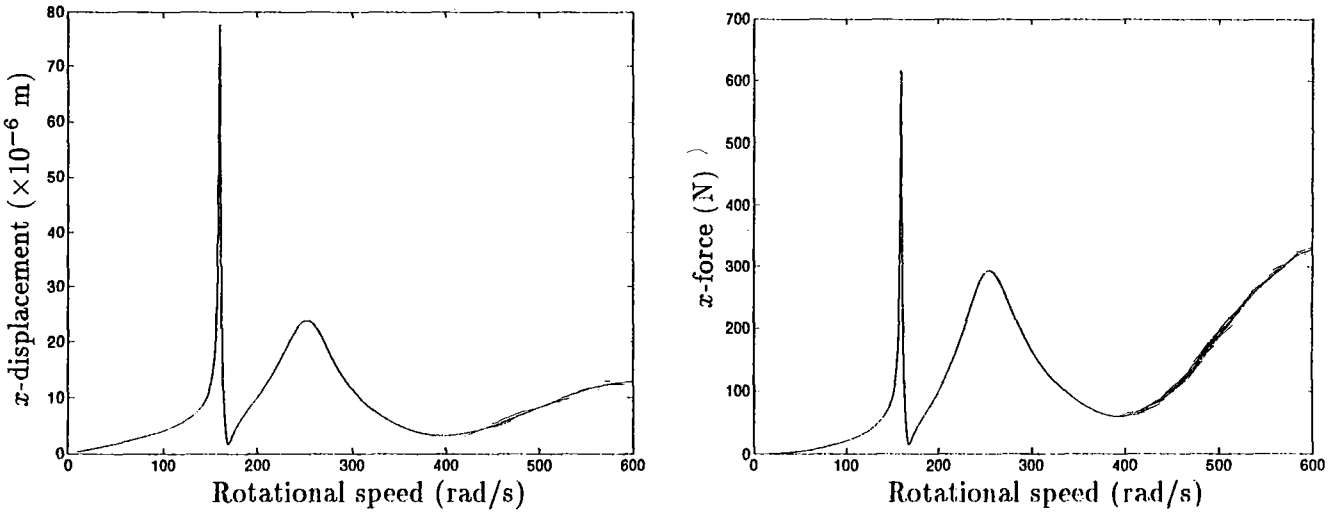

(b) High damping ($c_d = 5 \times 10^4$ Ns/m)

Figure 3. Linearized synchronous response amplitudes at non-driven end magnetic bearing in the x direction (45° to vertical against rotation) ($k_p = 1{\cdot}05k_z$, $k_z = 2{\cdot}05 \times 10^6$ N/m, $\tau = 10^{-3}$ s). The nominal unbalance was a 10 g mass on the rim of the non-driven end disk. The vibration controller of figure 2 is not present.

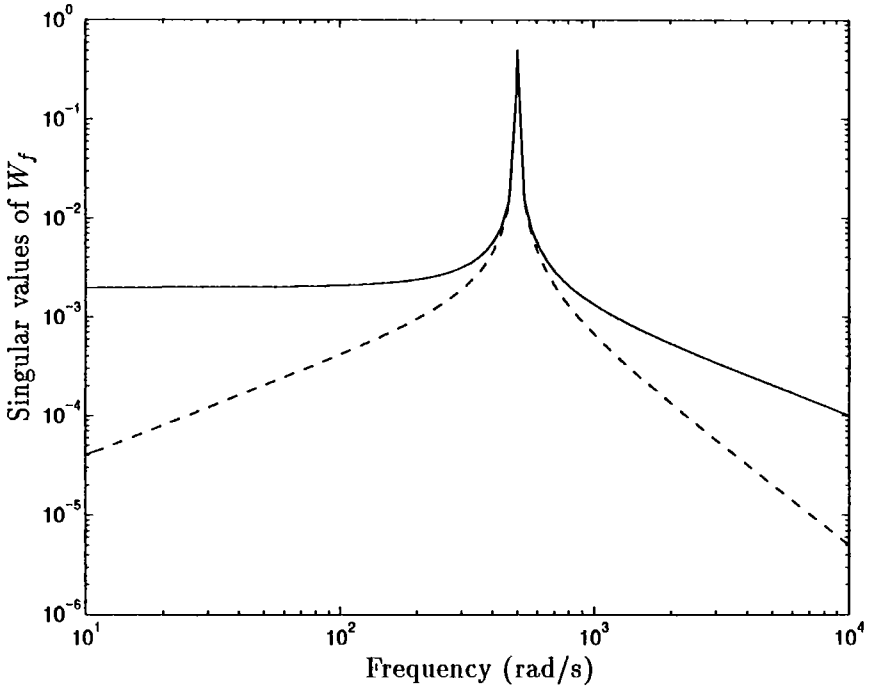

Figure 6. Singular values of weight function matrix $W_f(\mathrm{i}\omega)$.

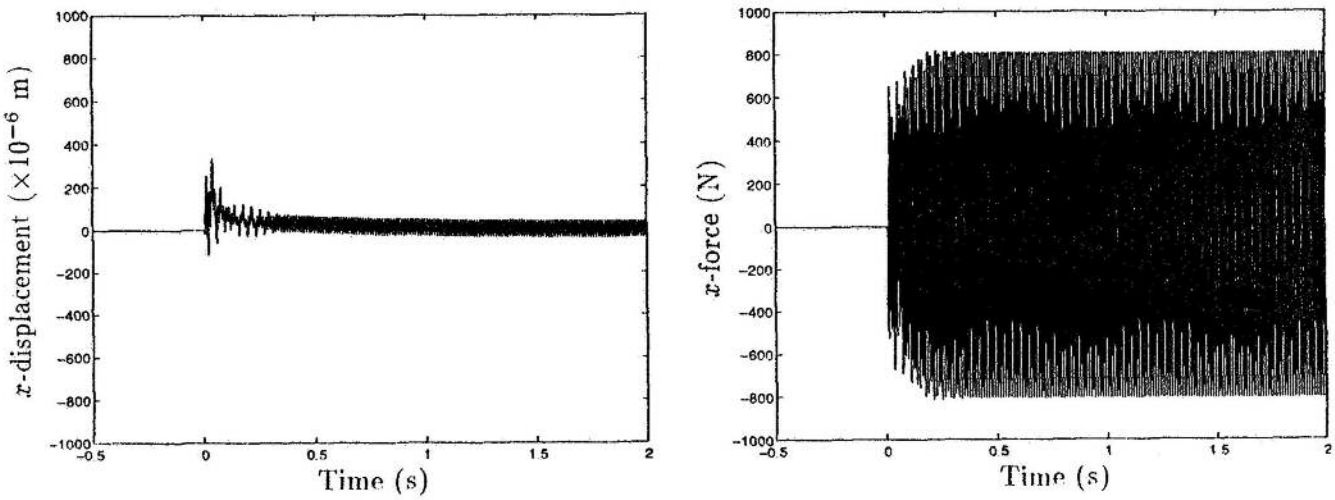

(a) Driven end magnetic bearing

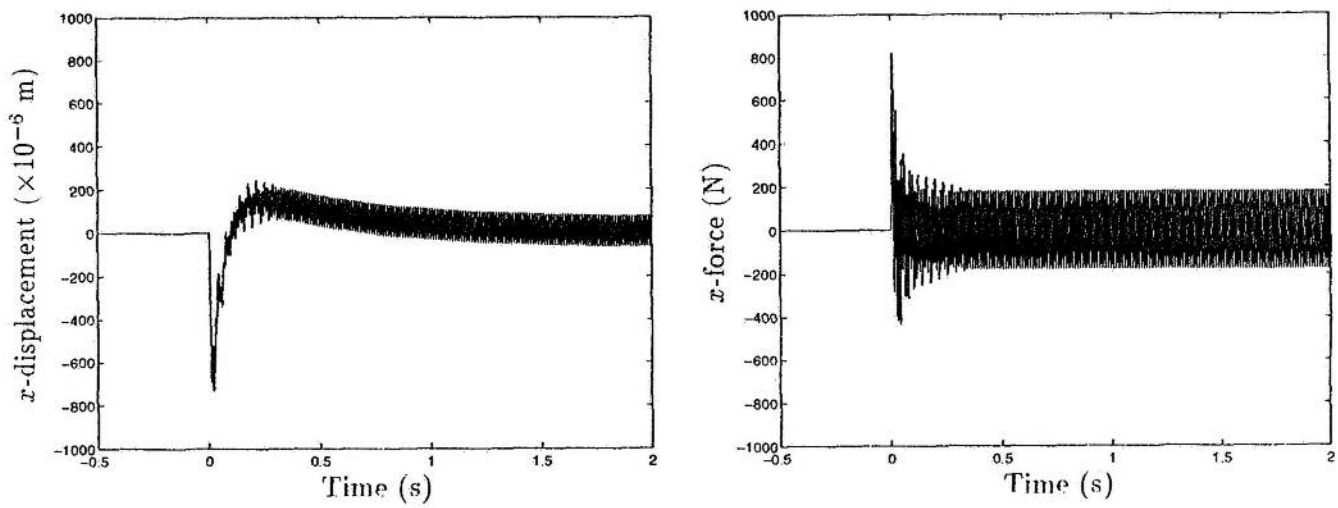

(b) Non-driven end magnetic bearing

Figure 7. Mass loss simulations at a speed $\Omega = 500$ rad/s with a 60 g mass removed from the non-driven end disk rim in the x direction at $t = 0$ ($k_p = 1{\cdot}05k_z$, $c_d = 7{\cdot}5\times10^3$ Ns/m, $k_z = 2{\cdot}05\times10^6$ N/m, $\tau = 10^{-3}$ s). Vibration components of rotor amplitude and bearing control force are shown at the magnetic bearings. Saturation force limits were set at 1000 and -1700 N. The vibration controller of figure 2 is present.